JOURNAL OF MATERIALS SCIENCE 21 (1986) 3339–3344

Accelerated spheroidization of hypoeutectoid steel by the decomposition of supercooled austenite

CHEN-CHIA CHOU, PO-WE KAO
Institute of Materials Science and Engineering, National Sun Yat-Sen University, Kaohsiung, Taiwan

GWO-HWA CHENG
R and D Department, China Steel Corporation, Kaohsiung, Taiwan

A thermal cycling treatment was used to produce a spheroidized structure of hypoeutectoid steel from direct decomposition of supercooled austenite. Scanning electron microscopy and quantitative metallography were employed to study the changing microstructure during the thermal cycling treatment. A conventional spheroidizing annealing was also investigated for comparison. It has been shown that the thermal cycling treatment results in a structure of cementite spheroidites homogeneously distributed in a ferrite matrix within a very short processing time, and the coarsening of cementite particles is controlled by the coupled diffusion of both carbon and iron atoms.

1. Introduction

To accelerate the spheroidizing of the pearlitic structure has long been the interest of the steel industry. The current available spheroidizing processes may be divided into four classes: (a) isothermal annealing at a temperature slightly below the A1 temperature [1, 2]; (b) thermal cycling near the A1 temperature [3, 4]; (c) isothermal annealing with the aid of prior cold work [5–8]; (d) hot deformation before, during or after the transformation of austenite to pearlite [9–12]. Recently several investigations [13, 14] have shown that a structure of spheroidized cementite and ferrite can be formed directly from the decomposition of supercooled austenite in a very short time. Instead of plastic deformation, a brief cooling cycle prior to the isothermal transformation of austenite was employed to introduce defects into the supercooled austenite, which may aid the nucleation of cementite particles and lead to a spheroidized structure. The complete thermal cycling process [13, 14] consists of austenitizing, and then rapidly quenching to a temperature slightly above the martensite transformation temperature (M_s), finally up-quenching to a temperature slightly below the A1 temperature for isothermal annealing.

Since this thermal cycling treatment [13, 14] has shown the feature of accelerating the spheroidization of pearlite, it is desirable to conduct further research on this subject. In the present work, scanning electron microscopy (SEM) and quantitative metallography were used to study the evolution and changing microstructure during this thermal cycling treatment. In addition, a conventional isothermal annealing was investigated for comparison.

2. Experimental procedure

Commercial AISI 1045 as-rolled steel bars were used in this study. The chemical compositions of the steels are shown in Table I and the information about their initial conditions are given in Table II. The heat treating procedures are shown in Table III, where "T" and "N" represent the thermal cycling treatment and the conventional isothermal annealing, respectively.

After heat treatment, the specimens were sectioned, polished and etched by 2% nital or picral to reveal the interior microstructure. Jeol JSM-35CF scanning electron microscope (SEM) was used for the microstructural observations.

According to previous work [1], it is reasonable to assume that the shape of the carbide is oblate. The major and minor axes of each particle were measured and grouped into size classes with over 1000 particles measured for each specimen, and the DeHoff analysis [15] for ellipsoids was used in this work. A Cambridge Quantimet 900 image analyser was used for quantitative metallographic analysis.

3. Results

The microstructure of the as-rolled steel bars used is shown in Fig. 1a, which is the typical hypoeutectoid structure consisting of pearlite and hypoeutectoid ferrite. The microstructural changing during the

TABLE I Chemical compositions (wt%)

Steel	C	Si	Mn	P	S	Cr	Al
A	0.45	0.27	0.67	0.015	0.012	0.014	0.026
B	0.46	0.23	0.76	0.012	0.013	0.014	0.009

0022–2461/86 $03.00 + .12

TABLE II Initial structure and properties

Steel	Specimen diameter (mm)	Interlamellar spacing (nm)	Hardness HV (200 g)	A1 temperature (K)
A	12	260	207 ± 6	994
B	5.5	260	245 ± 13	993

TABLE III Heat treating procedure

Designation	Steel	Procedure
N	A	Isothermal annealing at 973 K and air cooling
T	B	T-973K: austenitizing at 1223 K for 900 sec, quenching to a 603 K salt bath* and staying for 8 sec, then up-quenching to a 973 K lead bath for isothermal annealing and air cooling
		T-923K: the same as T-973K, but the isothermal annealing temperature changing to 923 K

*Composition of the salt bath : $NaNO_3$ (42%) + KNO_3 (58%).

isothermal annealing is illustrated in Figs 1b and c, while the evolution and changing of microstructure in the thermal cycling treatment is shown in Figs 1d to f. It is clearly shown that the T-973K treatment results in a structure of fine spheroidites homogeneously dispersed in the ferrite matrix after annealing for only 60 sec, however, the hypoeutectoid ferrite and cementite lamellae still persist in the conventional isothermal annealing (N) even after 6×10^3 sec.

Quantitative metallography was used to follow the progress of spheroidization of both treatments N and T-973K. Fig. 2 shows the aspect ratio distributions for both treatments N and T-973K, where the aspect ratio is the ratio of the minor axis to the major axis of the cementite particles. The peak of the aspect ratio distribution of the N treatment gradually shifts toward higher values with increasing annealing time, while a stable distribution is shown for the T-973K treatment. To assess the number percentage of spheroidization,

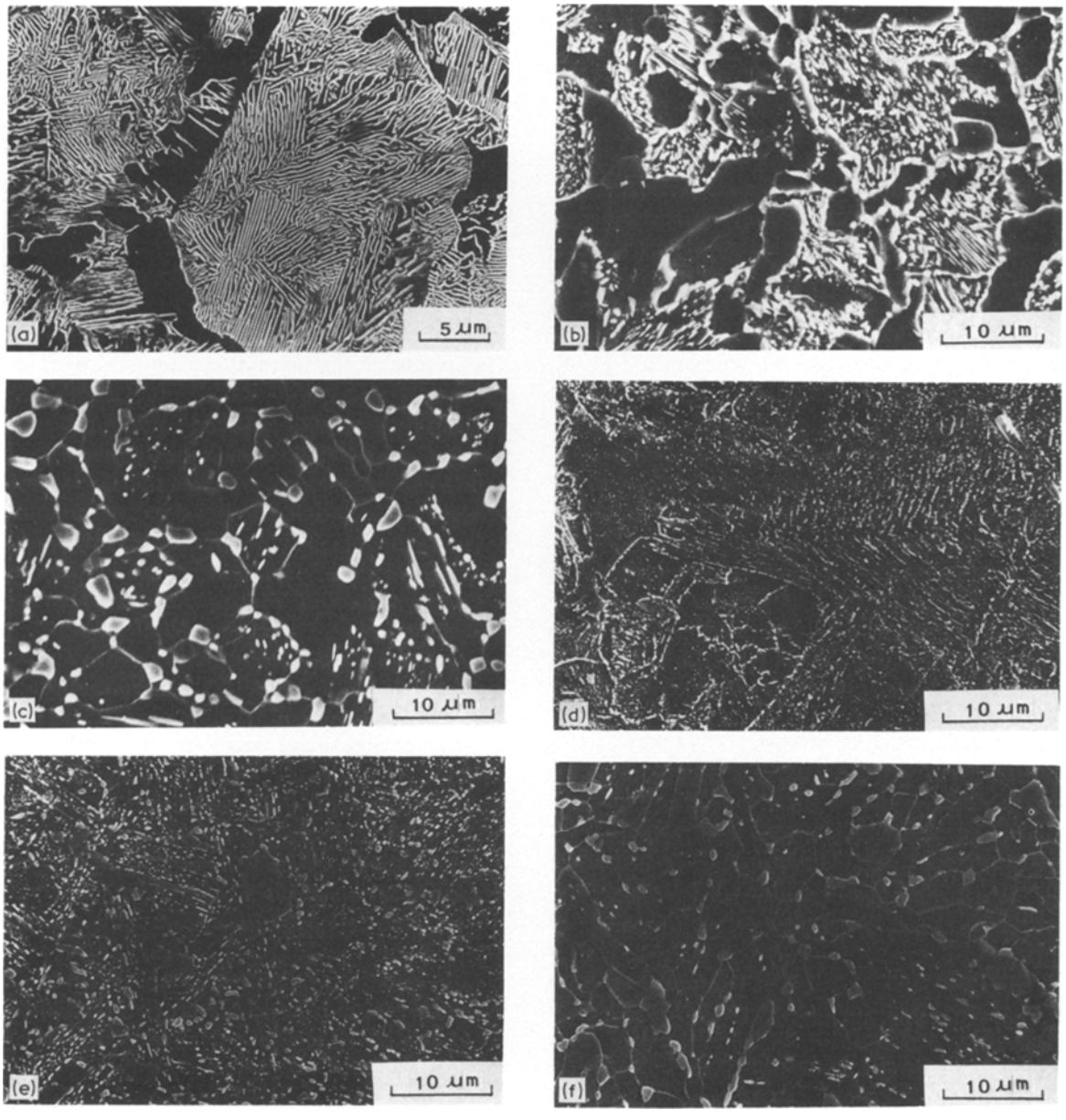

Figure 1 Scanning electron micrographs of (a) initial structure; (b) N treatment for 6×10^3 sec; (c) N treatment for 2.3×10^5 sec; (d) T-973K for 60 sec; (e) T-973K for 6×10^3 sec; (f) T-973K for 9.6×10^4 sec.

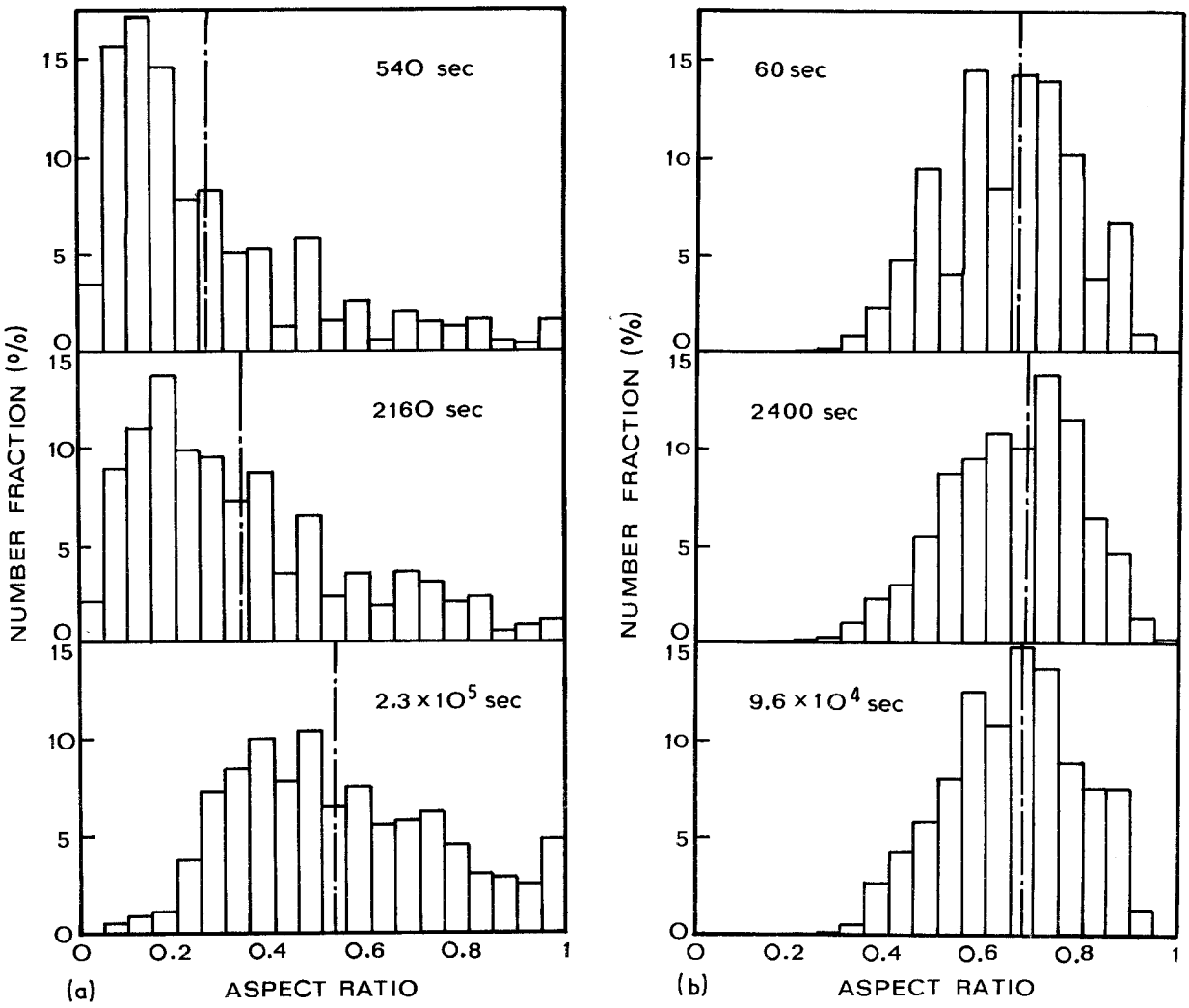

Figure 2 Aspect ratio distributions for (a) isothermal annealing (N) and (b) thermal cycling treatment (T-973K).

the criterion [2, 12], that particles of aspect ratio > 0.2 were considered as spheroidized, was employed in this work. According to the above criterion, Fig. 3 illustrates the change of percentage spheroidization with annealing time. It is indicated that for the N treatment, over 2×10^4 sec is needed to reach 100% spheroidization, however, less than 60 sec is necessary for T-973K treatment.

The number density of cementite particles is shown in Fig. 4 as a function of annealing time. The lower particle densities for the N treatment specimens are due to the larger size of the cementite particles in the initial pearlitic structure. It is worthwhile to notice the higher declining rate of the number density of particles in the T-973K treatment compared with the N treatment, which might indicate a more rapid softening

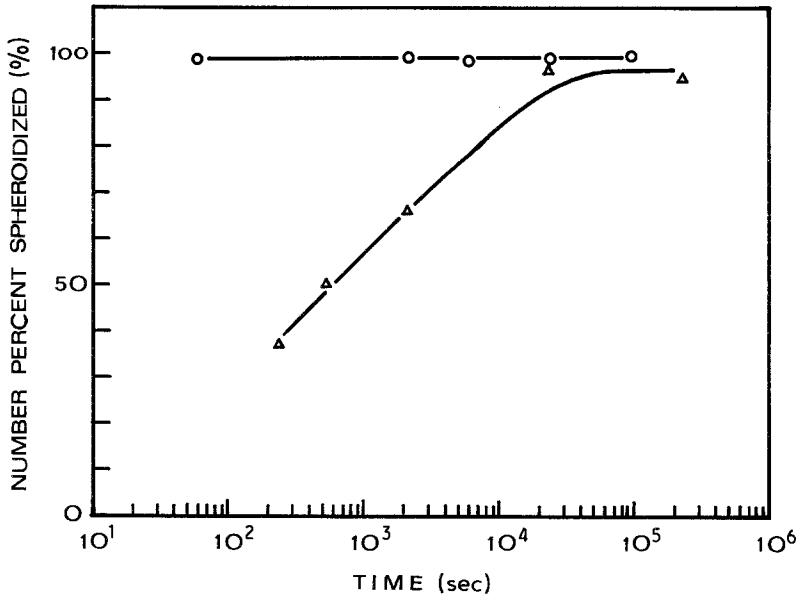

Figure 3 The change of percentage spheroidization with annealing time for both treatments N and T-973K. (○) T-973K; (△) N.

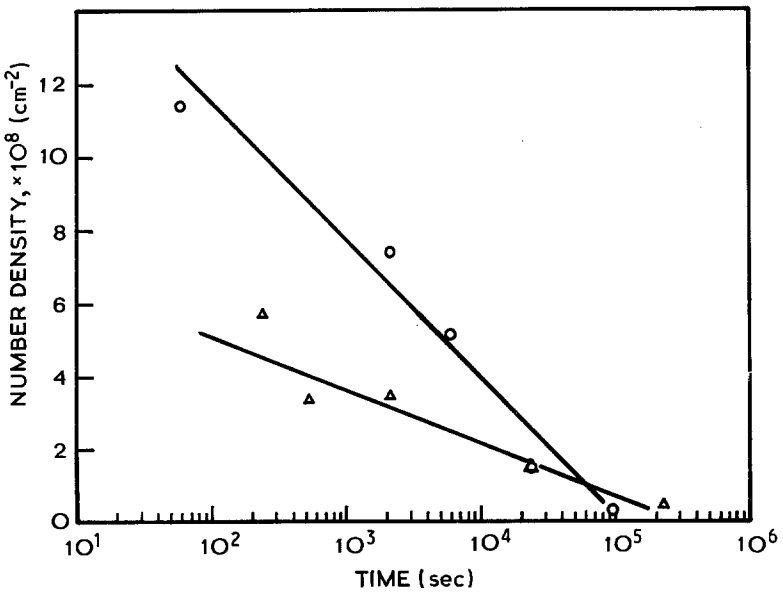

Figure 4 Number of cementite particles per unit area as a function of annealing time. (○) T-973K; (△) N.

rate associated with the T-973K treatment. The results shown in Figs 3 and 4 have indicated that the thermal cycling treatment reaches 100% spheroidization within a very short time and has a relatively fast decreasing rate of the number density of particles, therefore, it is necessary to investigate the growth of the particles in this treatment. The mean particle radius, $\bar{R}$, was determined for the T-973K specimens, and is plotted in the form of $(\bar{R}^3 - \bar{R}_0^3)$ as a function of $(t - t_0)$ (Fig. 5), where the $\bar{R}_0$ and t_0 values are taken from the shortest annealing time studied.

To understand better the thermal cycling treatment, a lower annealing temperature, 923 K, was applied in the T treatment. In general, both T-973K and T-923K treatments generate similar microstructures but the T-923K treatment results in finer cementite particles as shown in Fig. 6. The variation of hardness with the annealing time is shown in Fig. 7, where the T-923K treatment shows higher hardness values and lower softening rate compared with the T-973K treatment. In addition, a slightly higher softening rate is indicated for the T-973K treatment relative to the N treatment, which is consistent with the result shown in Fig. 4.

4. Discussion

As recognized by previous studies [2], spheroidization in the conventional isothermal annealing (N) involves break-up and coarsening of cementite lamellae. Fig. 8 shows the change of the major and minor axes of cementite particles as a function of annealing time, where L and S are the mean value of the major and minor axis, respectively. As spheroidization proceeds, the value of L of the treatment N first decreases as a result of break-up, and later the values of both L and S increase with annealing time which is a consequence of coarsening of the particles. On the other hand, a monotonic increase of both axes with increase of annealing time is shown in Fig. 8 for the thermal cycling treatment T-973K, which indicates coarsening of cementite particles. The aspect ratio distributions shown in Fig. 2 also support this conclusion.

The Lifshitz–Wagner [16, 17] theory predicts that, when the steady state size distribution of cementite particles is attained, the growth kinetics may be described by Equation 1 or 2:

(i) for diffusion-controlled growth

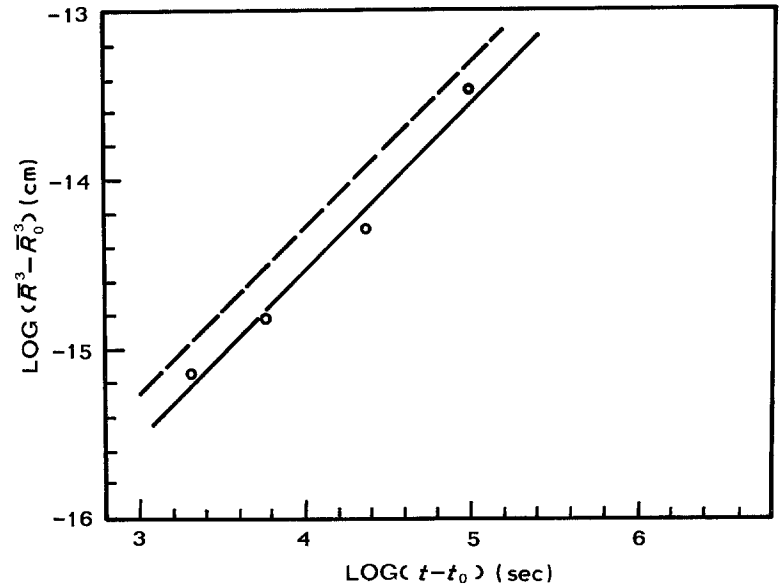

Figure 5 Variation of the mean particle radius, $\bar{R}$, with annealing time, t, plotted in the form of $(\bar{R}^3 - \bar{R}_0^3)$ as a function of $(t - t_0)$ for T-973K. (– – –) calculated; (○) T-973K.

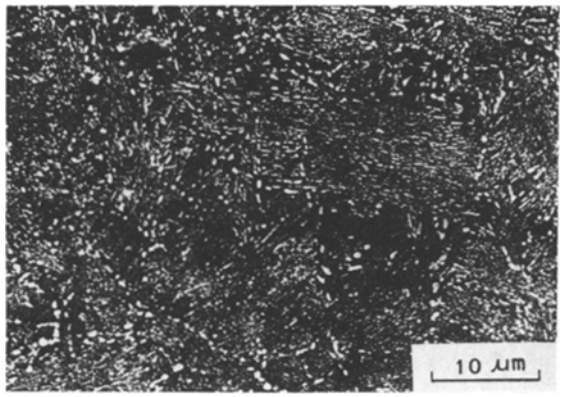

Figure 6 Scanning electron micrograph of T-923K–6 × 10^3 sec.

$$\bar{R}^3 - \bar{R}_0^3 = \frac{8\sigma D X_C V_{Fe_3C}^2}{9vRT}(t - t_0) \quad (1)$$

(ii) for interface-controlled growth

$$\bar{R}^2 - \bar{R}_0^2 = \frac{64kX_C V_{Fe_3C}^2}{81vRT}(t - t_0) \quad (2)$$

where $\bar{R}$ is the mean particle radius at any time t; $\bar{R}_0$ is the mean particle radius at time t_0; σ is the surface energy of the interface, assumed isotropic; D is the diffusion coefficient; X_C is the mole fraction of carbon in ferrite at steady state; R is the gas constant; T is the absolute temperature; k is the reaction constant; and v is the stoichiometric factor.

Li *et al.* [18] suggested that during coarsening of cementite there is a volume constraint which requires the diffusion of carbon as well as iron to take place. This leads to an effective coefficient for carbon, D_C^{eff}, which is given by

$$X_C D_C^{eff} = \frac{X_C D_C X_{Fe} D_{Fe}}{\left(\frac{V_{Fe_3C} - 3V_{Fe}}{V_{Fe}}\right)^2 X_C D_C + X_{Fe} D_{Fe}} \quad (3)$$

where X_C, X_{Fe}, are the mole fractions of carbon and iron in ferrite, D_{Fe} and D_C are the diffusion coefficients of iron and carbon in ferrite, and V_{Fe_3C}, V_C, V_{Fe} are the molar volumes of cementite, carbon and iron. By

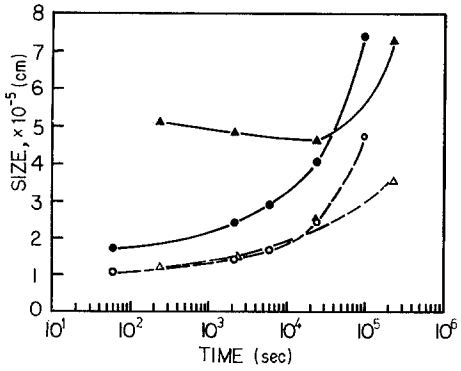

Figure 8 Change of the major and minor axis of cementite particles with annealing time. L and S are the mean of the major and minor axis, respectively. (●) L, T-973K; (▲) L, N; (○) S, T-973K; (△) S, N.

applying the effective diffusion coefficient, D_C^{eff}, Equation 1 can be given as [12]

$$\bar{R}^3 - \bar{R}_0^3 = \frac{8\sigma V_{Fe_3C}^2 (X_C D_C^{eff})}{9RTV_{Fe}}(t - t_0) \quad (4)$$

The growth data of the treatment T-973K presented in Fig. 5 were analysed according to Equation 4 and they fit the equation very well, in which the slope equals 1.0. The dashed line in Fig. 5 was calculated by using the following values for the variables in Equations 3 and 4. σ = 700 erg cm^{-2}, V_{Fe_3C} = 23.97 cm^3 mol^{-1}, V_{Fe} = 7.3 cm^3 mol^{-1} [19], X_C = 7.7 × 10^{-4} [20], X_{Fe} = 1, D_C = 8.7 × 10^{-7} cm^2 sec^{-1} [21], D_{Fe} = 6.3 × 10^{-14} cm^2 sec^{-1} [22]. As shown in Fig. 5, a good agreement was obtained between the results of T-973K and the calculated values. It can therefore be concluded that the coarsening of cementite particles in T-973K treatment is a diffusion controlled process. The effective diffusion coefficient of carbon for the T-973K treatment was found to be 6.3 × 10^{-10} cm^2 sec^{-1}, which is intermediate between D_C and D_{Fe}. A coupled diffusion coefficient of the type proposed by Li *et al.* [18] appears to be applicable in the coarsening process of the thermal cycling treatment.

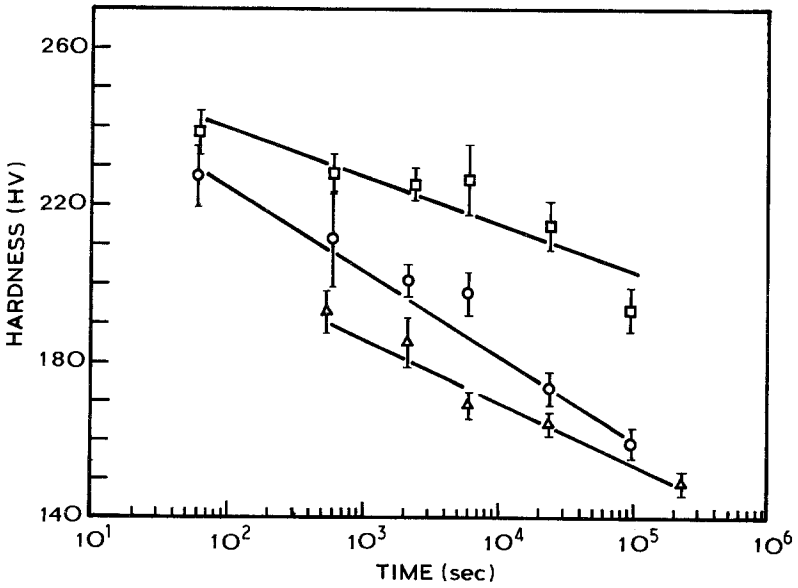

Figure 7 Variation of hardness with annealing time. (□) T-923K; (○) T-973K; (△) N.

As a result of eutectoid decomposition of austenite in carbon steels, pearlite comprising alternating plates of ferrite and cementite is usually formed. It is clearly shown in this work that the thermal cycling treatment results in an abnormal decomposition of austenite to a structure consisting of cementite spheroidites and ferrite. An experiment of the same thermal cycling treatment was interrupted after 8 sec at 603 K and quenched into ice water and only martensite was observed. It can therefore be concluded that a supercooled austenite was formed before the final upquench for isothermal annealing.

It is believed that considerable residual stresses must have been built up in the supercooled austenite by the thermal cycling (1223 → 603 → 973 or 923 K). To verify this suggestion, Parusov *et al.* [14] reported that a considerable magnitude of residual stresses were measured in an austenitic stainless steel after the thermal cycling treatment. In the course of thermal cycling austenite, an increase in dislocation densities results from the large thermal stresses. The dislocations in the austenite may aid the nucleation of cementite particles and lead to an abnormal decomposition of austenite, in consequence of which a spheroidized structure is formed.

To suppress the transformation of austenite during the cooling cycle (1223 → 603 K) and to build up enough thermal stresses are the keypoints for the success of the thermal cycling treatment. A 12 mm steel bar (steel A) was also processed by the same thermal cycling treatment and a structure comprising pearlite and hypoeutectoid ferrite was observed in the centre part of the bar. This observation indicates that the thermal cycling treatment has a limitation on the size or hardenability of steels to be processed.

5. Conclusions

1. An accelerated spheroidization of hypoeutectoid steel can be obtained from the thermal cycling treatment, which is a consequence of the abnormal decomposition of supercooled austenite.

2. It is suggested that the abnormal decomposition of austenite is due to the heterogeneous nucleation of cementite particles at dislocations, which are the results of thermal stresses caused by thermal cycling of austenite.

3. The coarsening of cementite particles in the thermal cycling treatment is a diffusion controlled process, and the effective diffusion coefficient agrees with the type proposed by Li *et al.* [18] which is the coupled diffusion of both carbon and iron atoms.

Acknowledgment

This research was supported by the China Steel Corporation.

References

1. K. M. VEDULA and R. W. HECKEL, *Metall. Trans.* **1** (1970) 9.
2. S. CHATTOPADHYAY and C. M. SELLARS, *Metallography* **10** (1977) 89.
3. P. PAYSON, W. I. HODPAPP and J. LEEDER, *Trans. ASM* **28** (1940) 306.
4. O. E. CULLEN, *Met. Prog.* **64** (1953) 79.
5. A. H. HOLTZMAN, J. C. DENKO and R. D. STOUT, *Trans. TSM-AIME* **212** (1958) 475.
6. M. KALDOR, *Acta Metall.* **10** (1962) 887.
7. D. F. LUPTON and D. H. WARRINGTON, *Met. Sci. J.* **6** (1972) 200.
8. D. GOODCHILD, *Scand. J. Metall.* **1** (1972) 235.
9. J. L. ROBBINS, O. C. SHEPARD and O. D. SHERBY, *J. Iron Steel Inst.* **202** (1964) 804.
10. O. D. SHERBY, M. J. HARRIGAN, L. CHAMAGNE and C. SAUVE, *Trans. ASM* **62** (1969) 575.
11. H. PAQUETON and A. PINEAU, *J. Iron Steel Inst.* **209** (1971) 991.
12. S. CHATTOPADHYAY and C. M. SELLARS, *Acta Metall.* **30** (1982) 157.
13. V. V. PARUSOV, I. I. DOLZHENKOV and M. F. EVSYUKOV, *Russ. Metall.* **3** (1978) 102.
14. V. V. PARUSOV, I. I. DOLZHENKOV, L. V. PODOBEDOV and I. A. VAKULENKO, *ibid.* **5** (1980) 143.
15. R. T. DEHOFF, *Trans. TMS-AIME* **224** (1962) 474.
16. I. M. LIFSHITZ and V. V. SLYOZOV, *Phys. Chem. Solids* **19** (1961) 35.
17. C. WAGNER, *Z. Electrochem.* **65** (1961) 581.
18. C. Y. LI, J. M. BLAKELY and A. H. FEINGOLD, *Acta Metall.* **14** (1966) 1397.
19. H. STUART and N. RIDLEY, *J. Iron Steel Inst.* **204** (1966) 711.
20. J. C. SWARTZ, *Trans. TMS-AIME* **245** (1969) 1083.
21. R. P. SMITH, *ibid.* **224** (1962) 195.
22. R. J. BORG and D. Y. F. LAI, *Acta Metall.* **9** (1961) 434.

Received 24 September
and accepted 25 November 1985